

# LIDAR AND TRUE-COLOR ORTHOPHOTOGRAPHS AIRBORNE DATA ACQUISITION AND PROCESSING: Grande Ronde Basin, OR

November, 2009

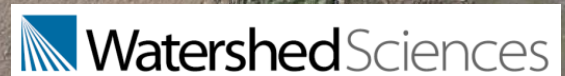
## Submitted to:

Lanie Paquin & Susan Fraser  
U.S. Department of the Interior  
Bureau of Reclamation  
1150 N Curtis Rd., Suite 100  
Boise, ID 83706-1234

## Submitted by:

Watershed Sciences  
257B SW Madison Ave.  
Corvallis, OR 97333

529 SW 3rd Ave. Suite 300  
Portland, Oregon 97204





# LIDAR AND TRUE-COLOR ORTHOPHOTOGRAPHS

## AIRBORNE DATA ACQUISITION AND PROCESSING: GRANDE RONDE BASIN, OR

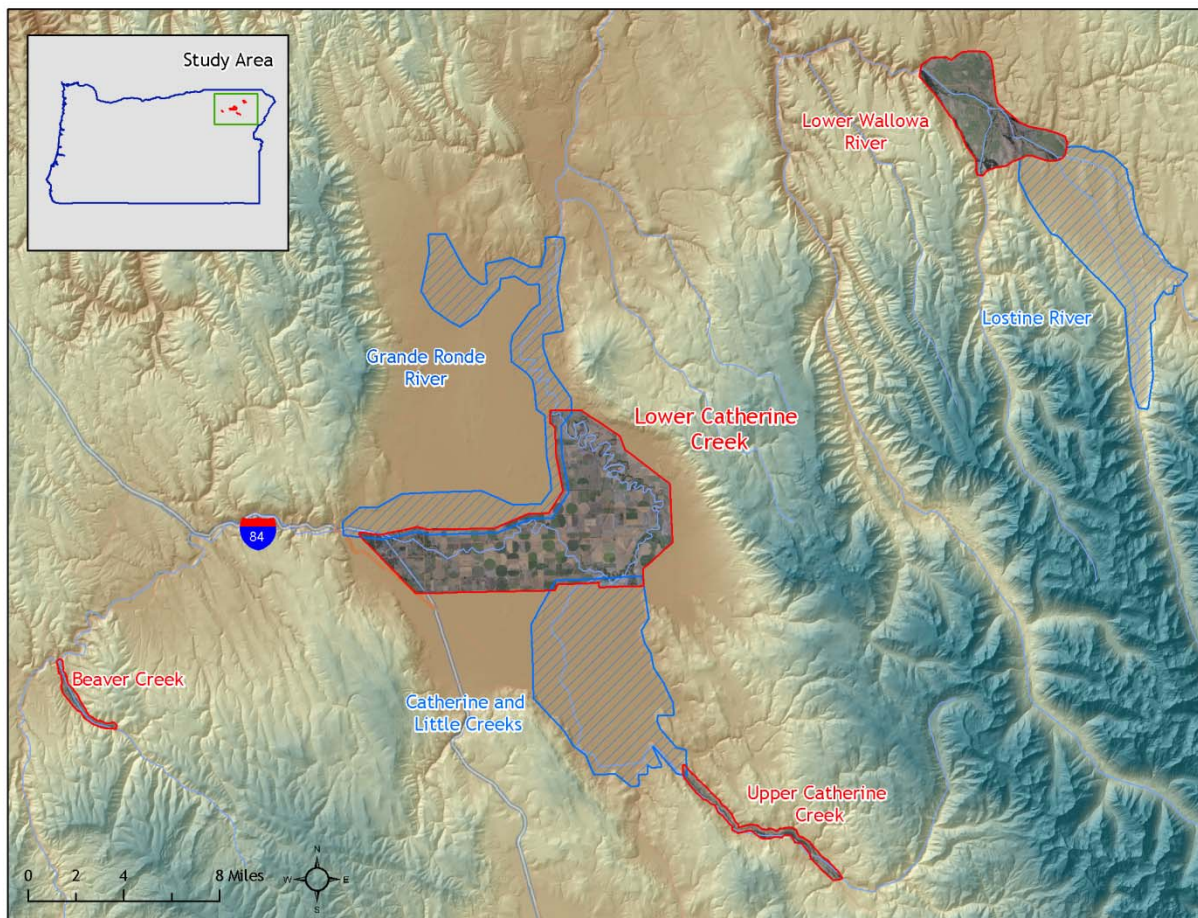
### TABLE OF CONTENTS

1. Overview .....	1
2. Acquisition .....	2
2.1 Airborne Survey - Instrumentation and Methods.....	2
2.2 Ground Survey - Instrumentation and Methods .....	3
2.2.1 Survey Control.....	3
2.2.2 RTK Survey.....	3
3. Data Processing.....	5
3.1 Applications and Work Flow Overview .....	5
3.2 Aircraft Kinematic GPS and IMU Data .....	6
3.3 Laser Point Processing .....	6
3.4 Orthophotograph Processing .....	7
4. LiDAR Accuracy Assessment .....	8
4.1 Laser Noise and Relative Accuracy.....	8
4.2 Absolute Accuracy .....	9
5. Photo Accuracy Assessment .....	9
6. Study Area Results .....	10
6.1 Data Summary .....	10
6.2 LiDAR Point Density/Resolution .....	10
6.3 LiDAR Relative Accuracy Calibration Results.....	13
6.4 LiDAR Absolute Accuracy .....	13
6.5 Orthophotograph Accuracy.....	15
6.6 Projection/Datum and Units .....	16
7. Deliverables.....	16
8. Selected Images.....	18
9. Glossary.....	21
Appendix A .....	22

# 1. Overview

Watershed Sciences, Inc. (WS) collected Light Detection and Ranging (LiDAR) data and true-color orthophotographs of the Grande Ronde Basin: a section of Catherine Creek connecting prior WS project areas in Catherine and Little Creeks with the Grand Ronde River; the Lower Wallowa River at the northern end of the prior WS project area of the Lostine River and Sheep Creek/Upper Grande Ronde River; and a section of Beaver Creek. LiDAR was collect from August 12<sup>th</sup> to 15<sup>th</sup>, 2009, and true-color images were collected on August 15<sup>th</sup> and 16<sup>th</sup>. This report contains information on the LiDAR and true-color orthophotograph data and analysis. The total area delivered is 42,198 acres (**Figure 1**). The requested area was expanded to include a 100 m buffer to ensure complete coverage and adequate LiDAR point densities around survey area boundaries.

*Figure 1. Grande Ronde Basin survey area. Previously delivered AOIs are outlined in blue, AOIs in this delivery are outlined in red.*



## 2. Acquisition

### 2.1 Airborne Survey - Instrumentation and Methods

The LiDAR survey used a Leica ALS50 Phase II laser system. For the Grande Ronde Basin survey area, the sensor scan angle was  $\pm 14^\circ$  from nadir<sup>1</sup> with a pulse rate designed to yield an average native density (number of pulses emitted by the laser system) of  $\geq 8$  points per square meter over terrestrial surfaces. All survey areas were surveyed with an opposing flight line side-lap of  $\geq 50\%$  ( $\geq 100\%$  overlap) to reduce laser shadowing and increase surface laser painting. The Leica ALS50 Phase II system allows up to four range measurements (returns) per pulse, and all discernable laser returns were processed for the output dataset.

The aerial imagery was collected using a Leica RCD-105 39 megapixel digital camera. For the Grande Ronde Basin survey area, images were collected in 3 spectral bands (red, green, blue) with 60% along track overlap and 30% sidelap between frames. The acquisition flight parameters were designed to yield native pixel resolution of  $\leq 6$  inches.



*The Cessna Caravan is a stable platform, ideal for flying slow and low for high density projects. The Leica ALS50 sensor head installed in the Caravan is shown on the left.*

To accurately solve for laser point position (geographic coordinates  $x, y, z$ ), the positional coordinates of the airborne sensor and the attitude of the aircraft were recorded continuously throughout the LiDAR and photo collection missions. Aircraft position was measured twice per second (2 Hz) by an onboard differential GPS unit. Aircraft attitude was measured 200 times per second (200 Hz) as pitch, roll and yaw (heading) from an onboard inertial measurement unit (IMU). To allow for post-processing correction and calibration, aircraft/sensor position and attitude data are indexed by GPS time.

---

<sup>1</sup> Nadir refers to the perpendicular vector to the ground directly below the aircraft. Nadir is commonly used to measure the angle from the vector and is referred to a “degrees from nadir”.

## 2.2 Ground Survey - Instrumentation and Methods

The following ground survey data were collected to enable the geo-spatial correction of the aircraft positional coordinate data collected throughout the flight, and to allow for quality assurance checks on final LiDAR data products.

### 2.2.1 Survey Control

Simultaneous with the airborne data collection mission, multiple static (1 Hz recording frequency) ground surveys were conducted over monuments with known coordinates in the Grande Ronde Basin survey area (Table 1). Indexed by time, these GPS data are used to correct the continuous onboard measurements of aircraft position recorded throughout the mission. Multiple sessions were processed over the same monument to confirm antenna height measurements and reported position accuracy. Controls were located within 13 nautical miles of the mission area(s).

*Trimble GPS survey equipment set up at the La Grande airport configured for collecting RTK data.*



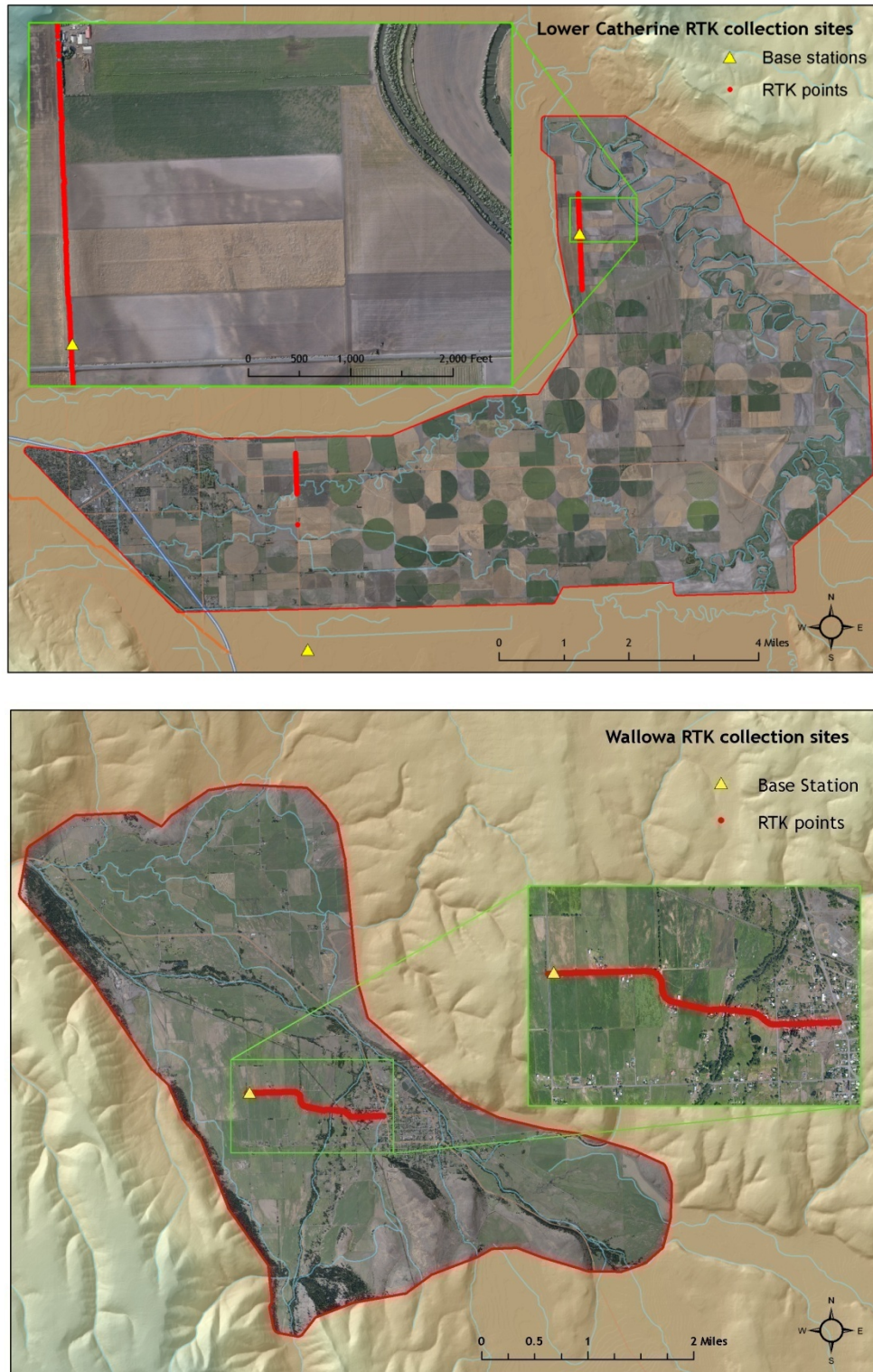
*Table 1. Base Station Survey Control coordinates for the Grande Ronde Basin survey area.*

Base Station ID	Datum: NAD83 (CORS91)		GRS80
	Latitude	Longitude	Ellipsoid Z (feet)
CRITFC_AXR1	45° 14' 54.86598"	118° 24' 30.32329"	1046.439
CATH_DB3	45° 17' 38.78430"	118° 0' 44.05939"	809393
CRITFC_TS1	45° 11' 43.15780"	117° 45' 41.27194"	1025.708
Cath_DB2	45° 23' 05.83916"	117° 55' 19.51159"	804.872
Wallowa_DB1	45° 34' 39.85120"	117° 33' 44.80119"	878.914

### 2.2.2 RTK Survey

To enable assessment of LiDAR data accuracy, ground truth points were collected using GPS based real-time kinematic (RTK) surveying. For an RTK survey, the ground crew uses a roving unit to receive radio-relayed corrected positional coordinates for all ground points from a GPS base station set up over a survey control monument. Instrumentation includes multiple Trimble DGPS units (R8). RTK surveying allows for precise location measurements with an error ( $\sigma$ ) of  $\leq 1.5$  cm (0.6 in). Figure 2 below portrays a distribution of RTK point locations used for the survey areas.

Figure 2. RTK and base station locations used for the Grande Ronde Basin survey area. Background image derived from a 10-m hillshade. AOI shape comprised of LiDAR highest-hit points overlaid with Orthophotographs.



## 3. Data Processing

### 3.1 Applications and Work Flow Overview

1. Resolved kinematic corrections for aircraft position data using kinematic aircraft GPS and static ground GPS data.  
**Software:** Waypoint GPS v.8.10, Trimble Geomatics Office v.1.62
2. Developed a smoothed best estimate of trajectory (SBET) file that blends post-processed aircraft position with attitude data. Sensor head position and attitude were calculated throughout the survey. The SBET data were used extensively for laser point processing.  
**Software:** IPAS v.1.4
3. Calculated laser point position by associating SBET position to each laser point return time, scan angle, intensity, etc. Created raw laser point cloud data for the entire survey in \*.las (ASPRS v1.1) format.  
**Software:** ALS Post Processing Software v.2.69
4. Imported raw laser points into manageable blocks (less than 500 MB) to perform manual relative accuracy calibration and filter for pits/birds. Ground points were then classified for individual flight lines (to be used for relative accuracy testing and calibration).  
**Software:** TerraScan v.9.001
5. Using ground classified points per each flight line, the relative accuracy was tested. Automated line-to-line calibrations were then performed for system attitude parameters (pitch, roll, heading), mirror flex (scale) and GPS/IMU drift. Calibrations were performed on ground classified points from paired flight lines. Every flight line was used for relative accuracy calibration.  
**Software:** TerraMatch v.9.001
6. Position and attitude data were imported. Resulting data were classified as ground and non-ground points. Statistical absolute accuracy was assessed via direct comparisons of ground classified points to ground RTK survey data. Data were then converted to orthometric elevations (NAVD88) by applying a Geoid03 correction. Ground models were created as a triangulated surface and exported as ArcInfo ESRI grids at a 3-ft pixel resolution.  
**Software:** TerraScan v.9.001, ArcMap v9.3, TerraModeler v.9.001
7. Converted raw images to tif format, calibrating raw image pixels for gain and exposure settings of each image.  
**Software:** Leica Calibration Post Processing v.1.0.4
8. Calculated photo position and orientation by associating the SBET position (Step 3) to each image capture time.  
**Software:** IPASCO v.1.3
9. Orthorectified calibrated tiffs utilizing photo orientation information (Step 8) and the LiDAR-derived ground surface (Step 6).  
**Software:** Leica Photogrammetry Suite v.9.2

10. To correct light imbalances between overlapping images, radiometric global tilting adjustments were applied to the rectified images.

**Software:** OrthoVista v.4.4.

11. The color corrected images were then mosaicked together for the survey area and subset into tiles to make the file size more manageable.

**Software:** OrthoVista v.4.4.

12. Mosaicked tiles were inspected for misalignments introduced by automatic seam generation. Misalignments were corrected by manual adjustments to seams.

**Software:** Adobe Photoshop 7.0, OrthoVista v.4.4.

### **3.2 Aircraft Kinematic GPS and IMU Data**

LiDAR survey datasets were referenced to the 1 Hz static ground GPS data collected over pre-surveyed monuments with known coordinates. While surveying, the aircraft collected 2 Hz kinematic GPS data, and the onboard inertial measurement unit (IMU) collected 200 Hz aircraft attitude data. Leica IPAS Suite was used to process the kinematic corrections for the aircraft. The static and kinematic GPS data were then post-processed after the survey to obtain an accurate GPS solution and aircraft positions. Waypoint was used to develop a trajectory file that includes corrected aircraft position and attitude information. The trajectory data for the entire flight survey session were incorporated into a final smoothed best estimated trajectory (SBET) file that contains accurate and continuous aircraft positions and attitudes.

### **3.3 Laser Point Processing**

Laser point coordinates were computed using the Leica ALS Post Processor software based on independent data from the LiDAR system (pulse time, scan angle), and aircraft trajectory data (SBET). Laser point returns (first through fourth) were assigned an associated (x, y, z) coordinate along with unique intensity values (0-255). The data were output into large LAS v. 1.2 files; each point maintains the corresponding scan angle, return number (echo), intensity, and x, y, z (easting, northing, and elevation) information.

These initial laser point files were too large for subsequent processing. To facilitate laser point processing, bins (polygons) were created to divide the dataset into manageable sizes (< 500 MB). Flightlines and LiDAR data were then reviewed to ensure complete coverage of the survey area and positional accuracy of the laser points.

Laser point data were imported into processing bins in TerraScan, and manual calibration was performed to assess the system offsets for pitch, roll, heading and scale (mirror flex). Using a geometric relationship developed by Watershed Sciences, each of these offsets was resolved and corrected if necessary.

LiDAR points were then filtered for noise, pits (artificial low points) and birds (true birds as well as erroneously high points) by screening for absolute elevation limits, isolated points and height above ground. Each bin was then manually inspected for remaining pits and birds and spurious points were removed. In a bin containing approximately 7.5-9.0 million points, an

average of 50-100 points are typically found to be artificially low or high. Common sources of non-terrestrial returns are clouds, birds, vapor, haze, decks, brush piles, etc.

Internal calibration was refined using TerraMatch. Points from overlapping lines were tested for internal consistency and final adjustments were made for system misalignments (i.e., pitch, roll, heading offsets and scale). Automated sensor attitude and scale corrections yielded 3-5 cm improvements in the relative accuracy. Once system misalignments were corrected, vertical GPS drift was then resolved and removed per flight line, yielding a slight improvement (<1 cm) in relative accuracy.

The TerraScan software suite is designed specifically for classifying near-ground points (Soininen, 2004). The processing sequence began by 'removing' all points that were not 'near' the earth based on geometric constraints used to evaluate multi-return points. The resulting bare earth (ground) model was visually inspected and additional ground point modeling was performed in site-specific areas to improve ground detail. This manual editing of grounds often occurs in areas with known ground modeling deficiencies, such as: bedrock outcrops, cliffs, deeply incised stream banks, and dense vegetation. In some cases, automated ground point classification erroneously included known vegetation (i.e., understory, low/dense shrubs, etc.). These points were manually reclassified as non-grounds. Ground surface rasters were developed from triangulated irregular networks (TINs) of ground points.

### **3.4 Orthophotograph Processing**

Image radiometric values were calibrated to specific gain and exposure settings associated with each capture using Leica's Calibration Post Processing software. The calibrated images were saved in tiff format to be used as inputs for the rectification process. Photo position and orientation was then calculated by assigning aircraft position and attitude information to each image by associating the time of image capture with trajectory file (SBET) in IPASCO. Photos were then orthorectified to the LiDAR derived ground surface using LPS. This typically results in <2 pixel relative accuracy between images. Relative accuracy can vary slightly with terrain but offsets greater than 2 pixels tend to manifest at the image edges which are typically removed in the mosaic process.

The rectified images were mosaicked together in a three step process using Orthovista. Firstly color correction was applied to each image using global tilting adjustments designed to homogenize overlapping regions. Secondly, discrepancies between images were minimized by an automated seam generation process. The most nadir portion of each image was selected and seams were drawn around landscape features. The requested tile delineation (1/16<sup>th</sup> USGS quads) was too large for the high-resolution orthophotos, therefore the orthophotos were re-delineated into a more manageable size (6500 ft x 6500 ft) appropriate to the pixel resolution and requested spatial reference.

## 4. LiDAR Accuracy Assessment

Our LiDAR quality assurance process uses the data from the real-time kinematic (RTK) ground survey conducted in the survey area. In this project, a total of 1230 RTK GPS measurements were collected on hard surfaces distributed among multiple flight swaths. To assess absolute accuracy, we compared the location coordinates of these known RTK ground survey points to those calculated for the closest laser points.

### 4.1 Laser Noise and Relative Accuracy

Laser point absolute accuracy is largely a function of laser noise and relative accuracy. To minimize these contributions to absolute error, we first performed a number of noise filtering and calibration procedures prior to evaluating absolute accuracy.

#### *Laser Noise*

For any given target, laser noise is the breadth of the data cloud per laser return (i.e., last, first, etc.). Lower intensity surfaces (roads, rooftops, still/calm water) experience higher laser noise. The laser noise range for this survey was approximately 0.02 meters.

#### *Relative Accuracy*

Relative accuracy refers to the internal consistency of the data set - the ability to place a laser point in the same location over multiple flight lines, GPS conditions, and aircraft attitudes. Affected by system attitude offsets, scale, and GPS/IMU drift, internal consistency is measured as the divergence between points from different flight lines within an overlapping area. Divergence is most apparent when flight lines are opposing. When the LiDAR system is well calibrated, the line-to-line divergence is low (<10 cm). See Appendix A for further information on sources of error and operational measures that can be taken to improve relative accuracy.

#### **Relative Accuracy Calibration Methodology**

1. **Manual System Calibration:** Calibration procedures for each mission require solving geometric relationships that relate measured swath-to-swath deviations to misalignments of system attitude parameters. Corrected scale, pitch, roll and heading offsets were calculated and applied to resolve misalignments. The raw divergence between lines was computed after the manual calibration was completed and reported for each survey area.
2. **Automated Attitude Calibration:** All data were tested and calibrated using TerraMatch automated sampling routines. Ground points were classified for each individual flight line and used for line-to-line testing. System misalignment offsets (pitch, roll and heading) and scale were solved for each individual mission and applied to respective mission datasets. The data from each mission were then blended when imported together to form the entire area of interest.
3. **Automated Z Calibration:** Ground points per line were utilized to calculate the vertical divergence between lines caused by vertical GPS drift. Automated Z calibration was the final step employed for relative accuracy calibration.

## 4.2 Absolute Accuracy

The vertical accuracy of the LiDAR data is described as the mean and standard deviation (sigma -  $\sigma$ ) of divergence of LiDAR point coordinates from RTK ground survey point coordinates. To provide a sense of the model predictive power of the dataset, the root mean square error (RMSE) for vertical accuracy is also provided. These statistics assume the error distributions for x, y, and z are normally distributed, thus we also consider the skew and kurtosis of distributions when evaluating error statistics.

Statements of statistical accuracy apply to fixed terrestrial surfaces only and may not be applied to areas of dense vegetation or steep terrain. To calibrate laser accuracy for the LiDAR dataset 1230 RTK points were collected on fixed, hard-packed road surfaces within the survey area.

## 5. Photo Accuracy Assessment

To assess spatial accuracy of the orthophotographs they are compared against control points identified from the LiDAR intensity images. The control points were collected and measured on surface features such as painted road-lines, and boulders in the stream beds. The accuracy of the final mosaic, expressed as root mean square error (RMSE), was calculated in relation to the LiDAR-derived control points. **Figure 3** displays the co-registration between orthorectified photographs and LiDAR intensity images.

*Figure 3. Example of co-registration of color images with LiDAR intensity images in GRB study area.*



## 6. Study Area Results

Summary statistics for point resolution and accuracy (relative and absolute) of the LiDAR data collected in the Grande Ronde Basin survey area are presented below in terms of central tendency, variation around the mean, and the spatial distribution of the data (for point resolution by bin).

### 6.1 Data Summary

Table 2. LiDAR Resolution and Accuracy - Specifications and Achieved Values

	Targeted	Achieved
<b>Resolution:</b>	$\geq 8 \text{ points/m}^2$	7.23 points/m <sup>2</sup> * (0.7 points/ft <sup>2</sup> )
<b>Vertical Accuracy (1 <math>\sigma</math>):</b>	$\leq 15 \text{ cm}$	5.3 cm (0.17ft)

\* Differences ( $\pm$ ) between the 'native' and 'delivered' density are frequently observed due to terrain relief, types of land cover, prevalence of water bodies, and filtering of the raw data. Some types of surfaces (e.g. dense vegetation, dark pavement, or water) have low reflectivity and ultimately return fewer pulses than the laser originally emitted. In addition, the raw laser returns are filtered during the data processing to remove spurious points and edge effects in order to improve overall data quality. In this case, the "achieved" pulse density was on average slightly below the targeted density.

Table 3. Photo Resolution and Accuracy - Specifications and Achieved Values

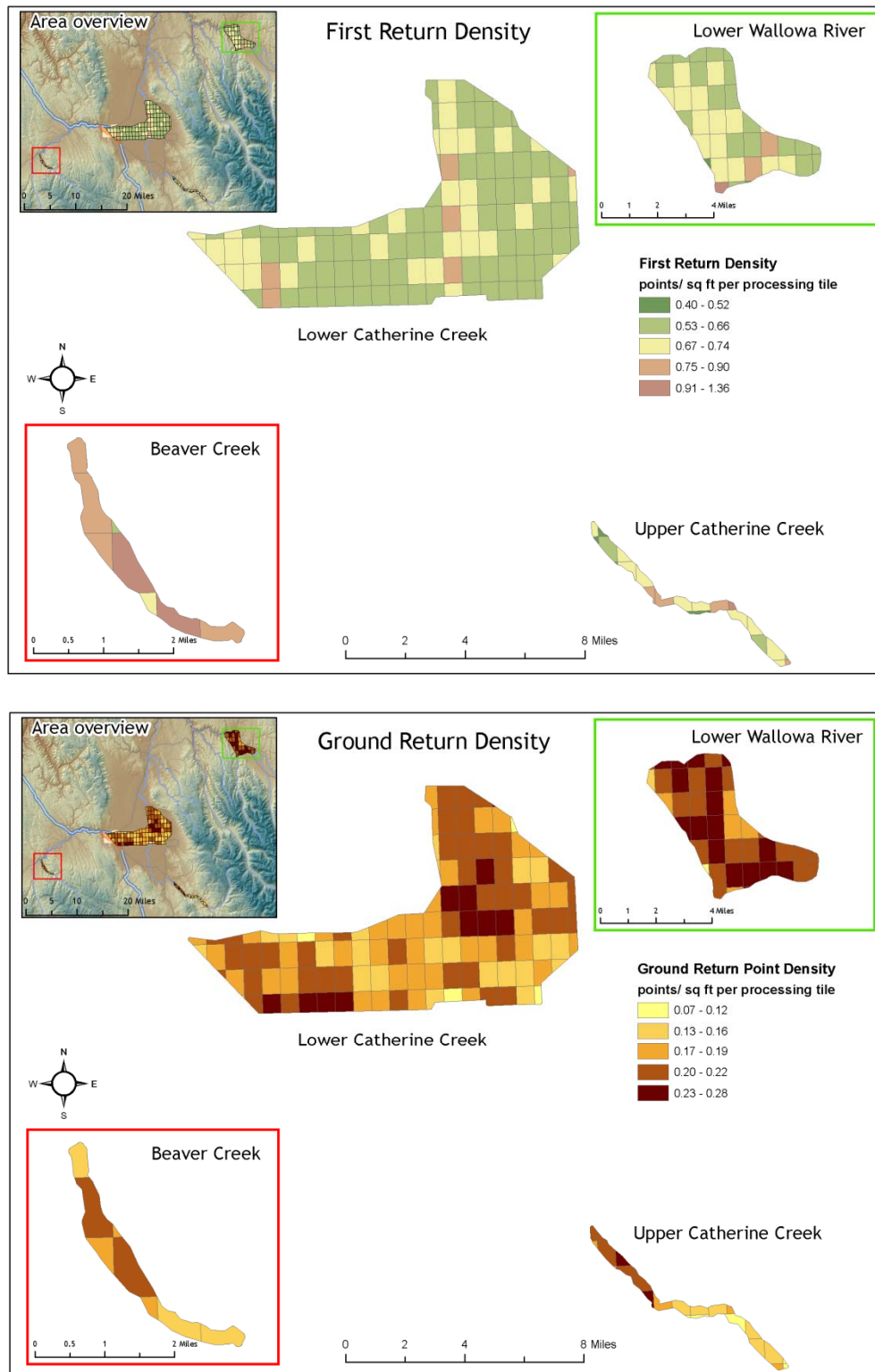
	Targeted	Achieved
<b>Resolution:</b>	$\leq 6 \text{ in}$	6 in
<b>Horizontal Accuracy (1 <math>\sigma</math>)</b>	$\leq 45 \text{ cm}$	0.93ft (28cm)

### 6.1 LiDAR Point Density/Resolution

Ground classifications were derived from automated ground surface modeling and manual, supervised classifications where it was determined that the automated model had failed. Ground return densities will be lower in areas of dense vegetation, water, or buildings.

Figure 4 (below) displays the spatial distribution of first-return and ground-classified point densities per processing tile.

Figure 4. Density distribution for first-return and ground-classified laser point densities per 1/100<sup>th</sup> USGS quad.



Data resolution for the Grande Ronde Basin survey area:

- Average Point (First Return) Density = 0.67 points/ft<sup>2</sup> (7.23 points/m<sup>2</sup>)
- Average Ground Point Density = 0.19 points/ft<sup>2</sup> (2.03 points/m<sup>2</sup>)

Figure 5. Density distribution for first return laser points

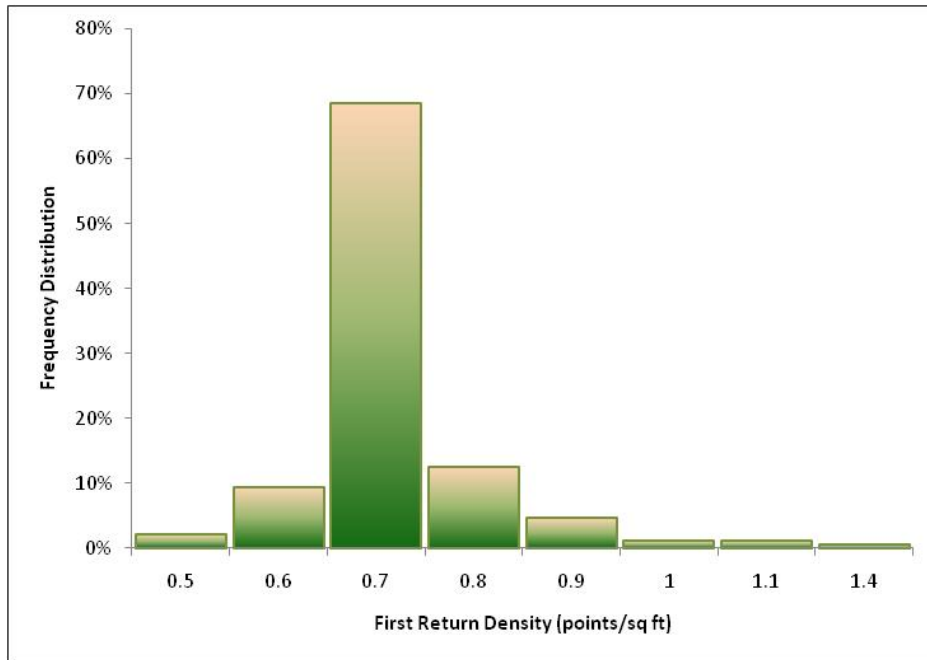
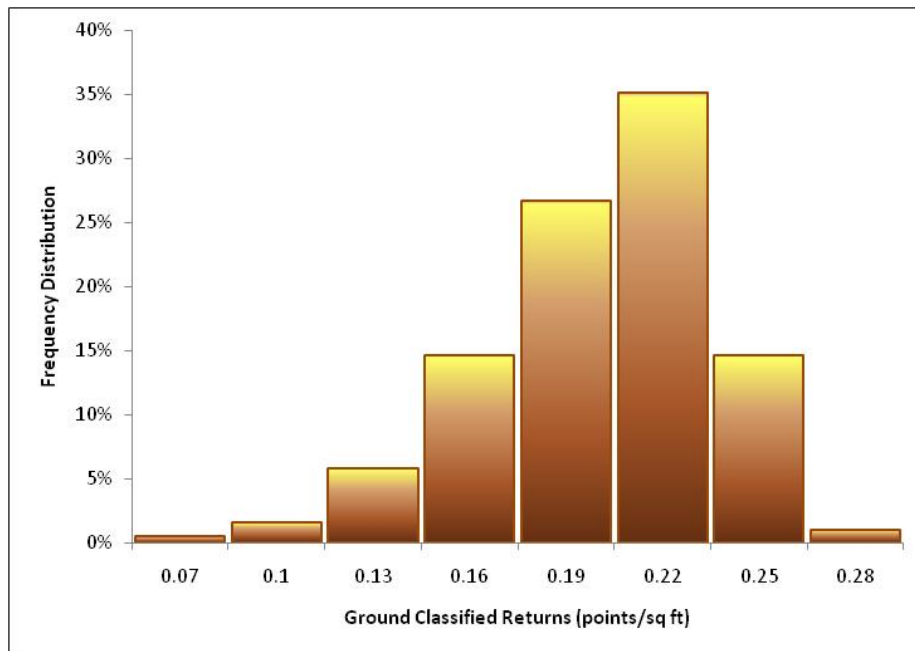


Figure 6. Density distribution for ground-classified laser points

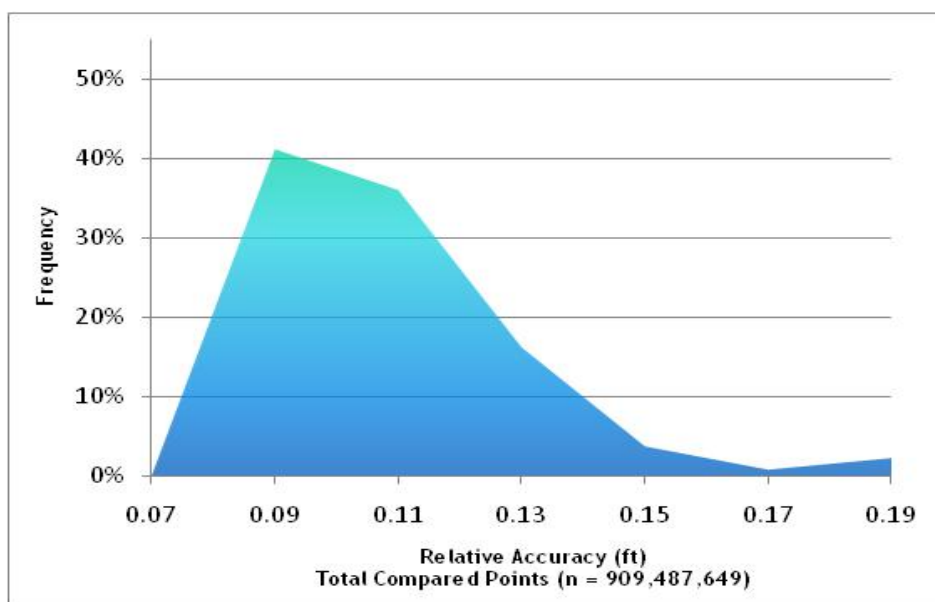


### 6.3 LiDAR Relative Accuracy Calibration Results

Relative accuracies for the Grande Ronde Basin survey area:

- Project Average = 0.095ft
- Median Relative Accuracy = 0.092ft
- 1 $\sigma$  Relative Accuracy = 0.096ft
- 2 $\sigma$  Relative Accuracy = 0.136ft

Figure 7. Distribution of relative accuracies per flight line, non slope-adjusted



### 6.4 LiDAR Absolute Accuracy

Absolute accuracies for Grande Ronde Basin survey area:

Table 4. Absolute Accuracy - Deviation between laser points and RTK hard surface survey points

RTK Survey Sample Size (n): 1230	
Root Mean Square Error (RMSE) = 0.09ft (0.03m)	Minimum $\Delta z$ = -1.3ft (-0.4m)
Standard Deviations 1 sigma ( $\sigma$ ): 0.08ft (0.02m)      2 sigma ( $\sigma$ ): 0.17ft (0.05m)	Maximum $\Delta z$ = 0.32ft (0.1m)
	Average $\Delta z$ = -0.003ft (0.001m)

Figure 8. Absolute Accuracy - Histogram Statistics, based on hard surface points

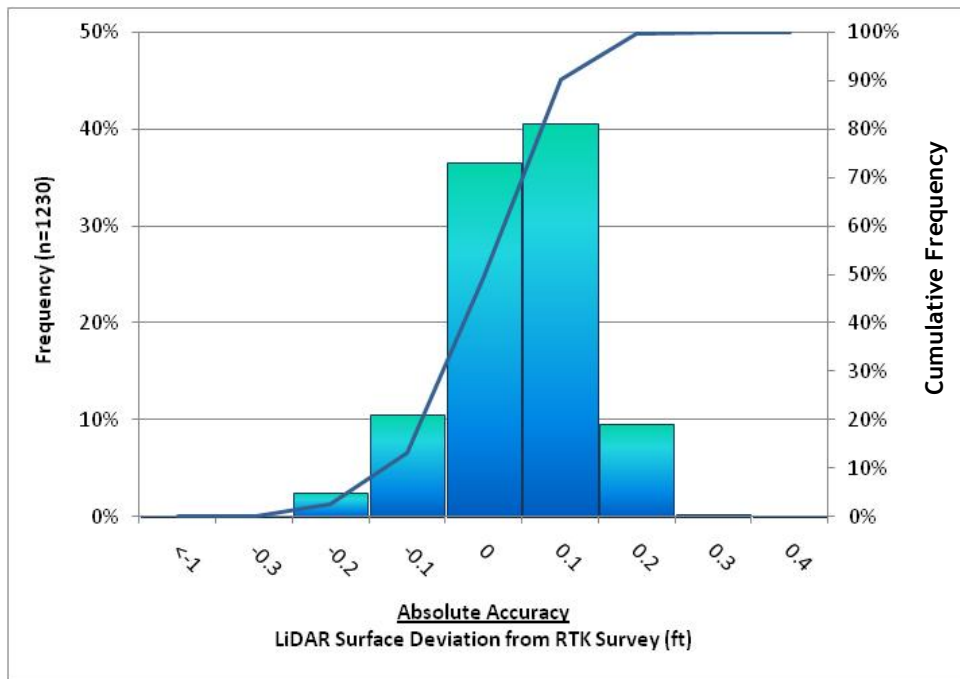
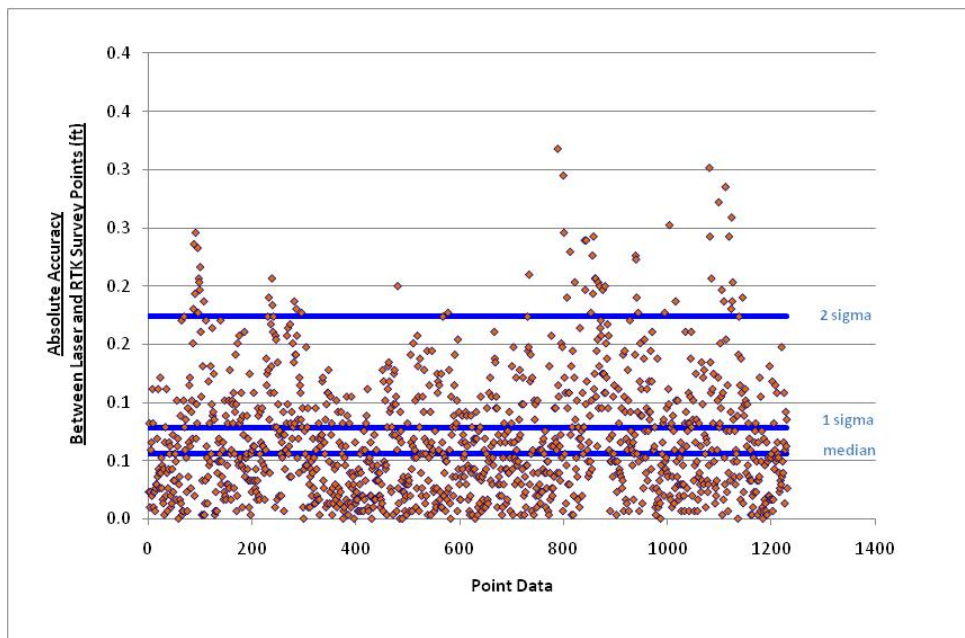


Figure 9. Absolute Accuracy - Absolute Deviation, based on hard surface points



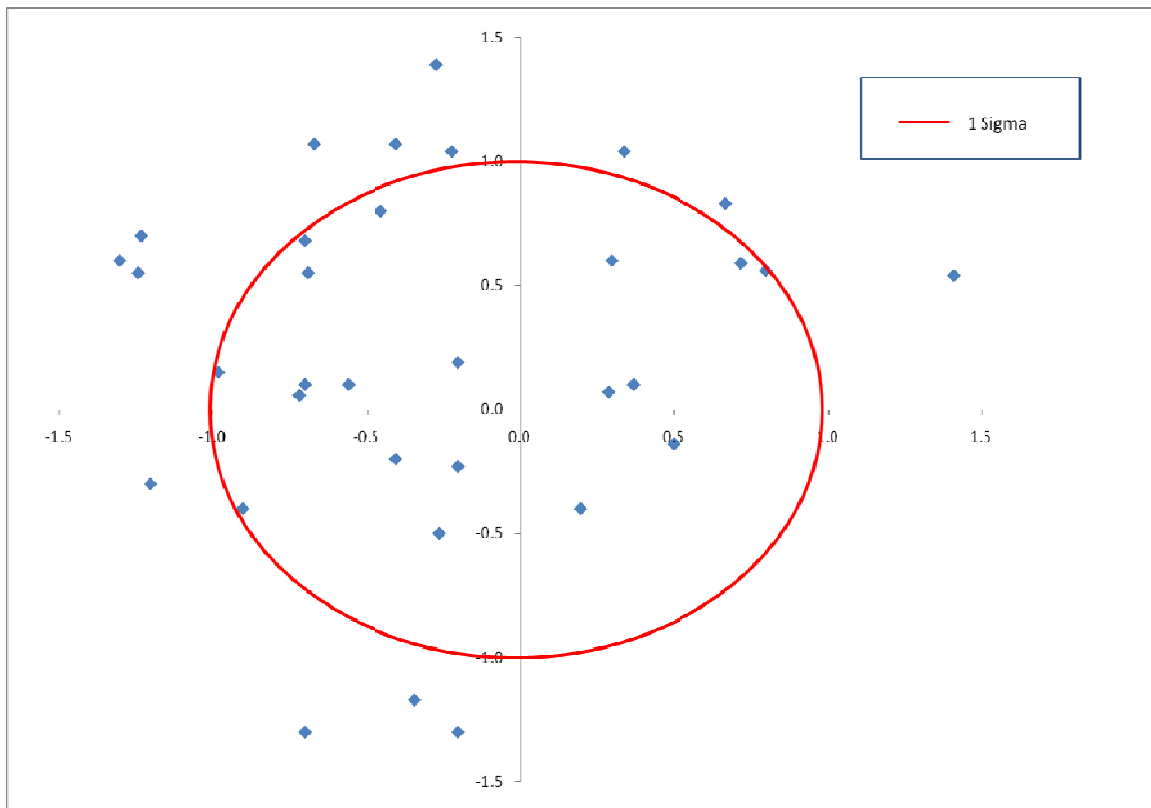
## 6.5 Orthophotograph Accuracy

Aerial imagery accuracy for the Grande Ronde Basin survey area is found in figure 10 and table 5 below.

Table 5. Deviation between aerial photos and intensity images based on 45 accuracy check points.

	Mean	Standard Deviation (1 Sigma)	Root Mean Square Error (RMSE)
GRB Photos	0.42ft (0.13m)	1.00ft (0.30m)	1.08ft (0.33m)

Figure 10. Checkpoint residuals derived from comparing aerial photos to intensity images



## 6.6 Projection/Datum and Units

<b>Projection:</b>		Oregon State Plane
<b>Datum</b>	<b>Vertical:</b>	NAVD88 Geoid03
	<b>Horizontal:</b>	NAD83
<b>Units:</b>		International Feet

## 7. Deliverables

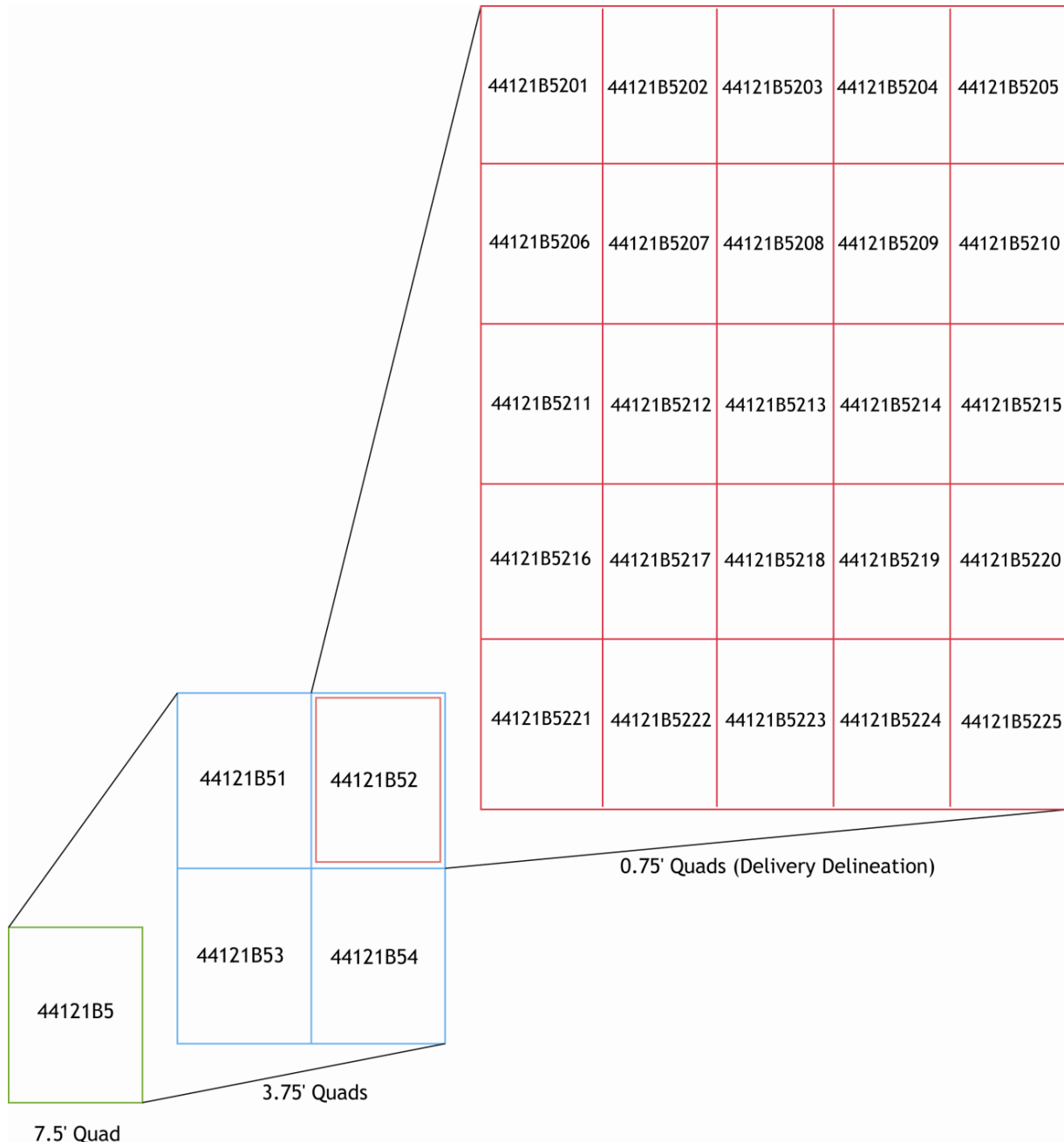
<b>Point Data:</b>	<ul style="list-style-type: none"> <li>• All laser return points (LAS v. 1.2 and ASCII formats; 1/100<sup>th</sup> USGS quad delineation)</li> <li>• First return points (LAS v. 1.2 and ASCII formats; 1/100<sup>th</sup> USGS quad delineation)</li> <li>• Ground classified points (LAS v. 1.2 and ASCII formats; 1/100<sup>th</sup> USGS quad delineation)</li> </ul>
<b>Vector Data:</b>	<ul style="list-style-type: none"> <li>• 2-ft Contours (dxf format; 1/100<sup>th</sup> USGS quad delineation)</li> <li>• LiDAR tile index (shapefile format)</li> <li>• Orthophoto tile index (shapefile format)</li> </ul>
<b>Raster Data:</b>	<ul style="list-style-type: none"> <li>• Intensity Images (1.5-ft GeoTIFF format; 1/100<sup>th</sup> USGS quad delineation)</li> <li>• Bare-Earth Model (3-ft ESRI GRID format; 1/4<sup>th</sup> USGS quad delineation)</li> <li>• Highest-Hit Model (3-ft-m ESRI GRID format; 1/4<sup>th</sup> USGS quad delineation)</li> <li>• Orthorectified True Color Imagery (8-bit/GeoTIFF format, Orthophoto tile index)</li> </ul>
<b>Data Report:</b>	<ul style="list-style-type: none"> <li>• Full Report containing introduction, methodology, and accuracy</li> </ul>

## Point Data (per 1/100th USGS Quad delineation\*)

- LAS v1.2 or ASCII Format

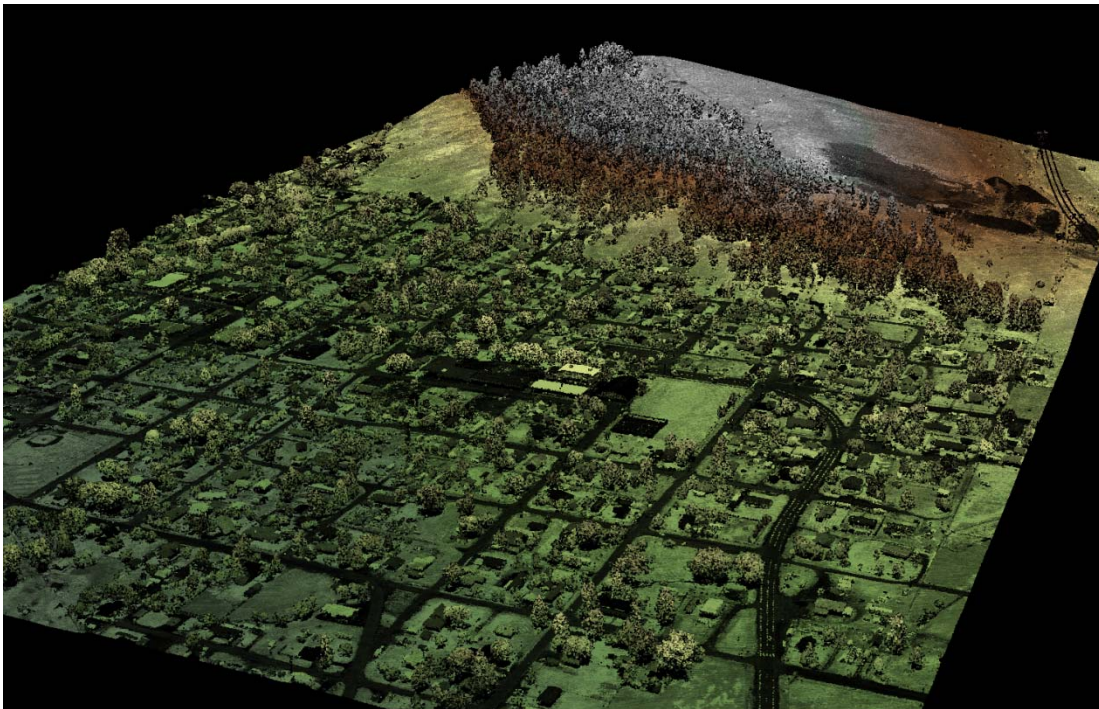
\*Note: Delineation based on 1/100<sup>th</sup> of a full 7.5-minute USGS Quad (.075-minutes). Larger delineations, such as 1/64<sup>th</sup> USGS Quads, resulted in unmanageable file sizes due to high data density.

Figure 11. Quadrangle naming convention for 1/100th of a 7.5-minute USGS Quad.

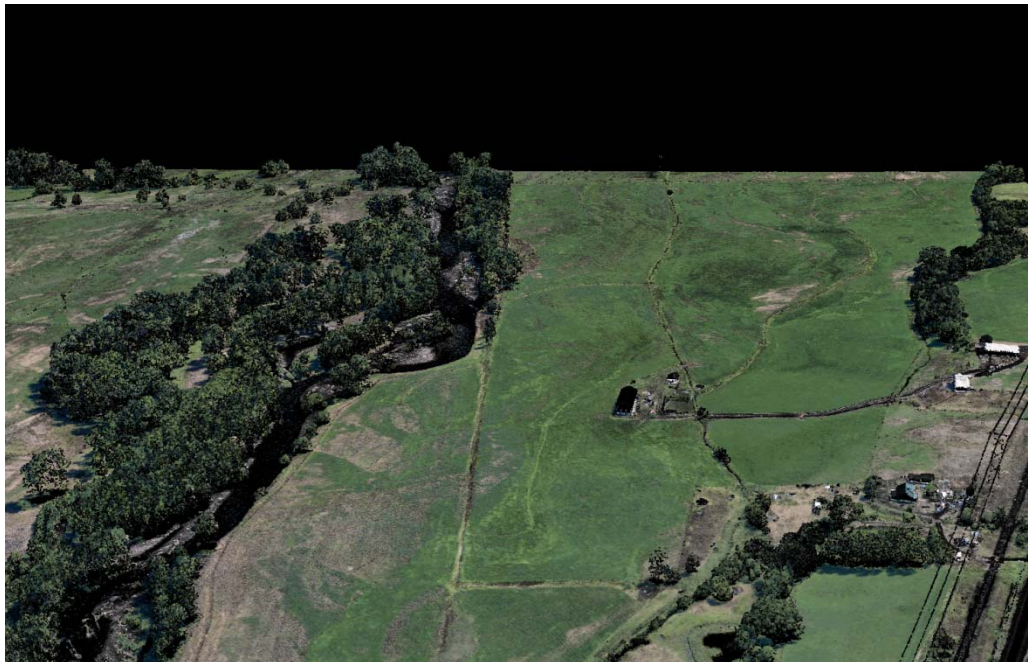


## 8. Selected Images

*Figure 12. 3-d oblique looking south over the town of Wallowa, Oregon. Image is derived from LiDAR point cloud colored by intensity.*



*Figure 13. View looking east, upstream along Wallowa River and utility corridor in Diamond Prairie area. Image Derived from LiDAR Point Cloud colored by orthophotographs.*



LiDAR and True-color Orthophotographs, Airborne Data Acquisition and Processing: Grande Ronde Basin, OR  
Prepared by Watershed Sciences, Inc.

*Figure 14. View of the confluence of Bear Creek and the Wallowa River, with Oregon State Route 82 running along east side and utility corridor running diagonally in southwestern portion of image. Image is derived from highest-hit LiDAR points colored by orthophotographs.*



*Figure 15. Top view looking Southwest down Beaver Creek and bottom view looking North up Beaver Creek. Image Derived from LiDAR Point Cloud colored by orthophotographs.*

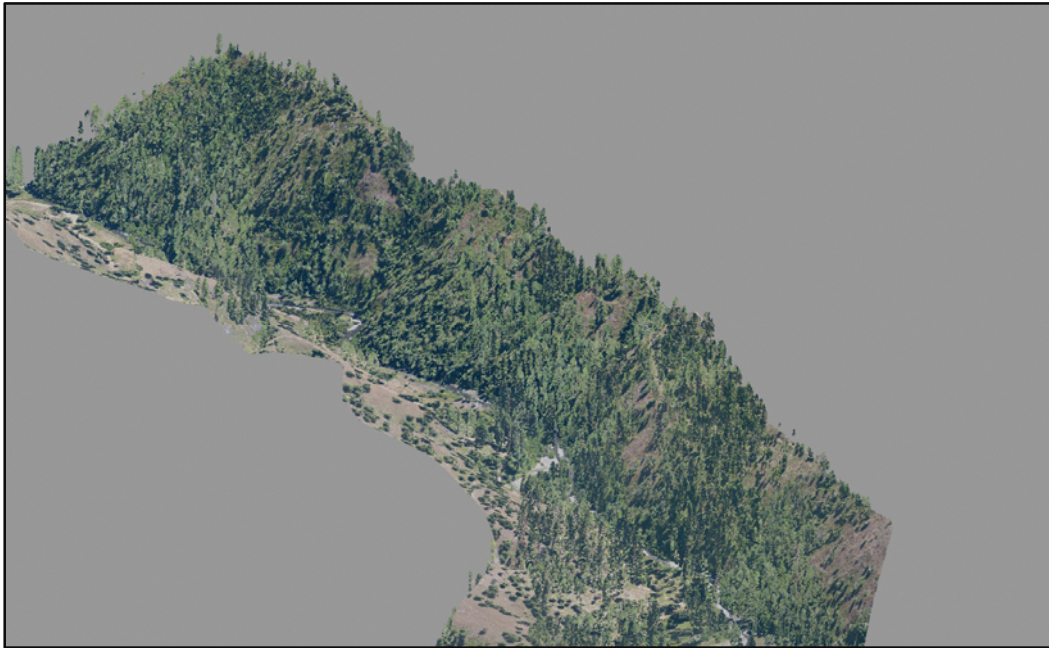


*Figure 16. View looking east, upstream along Wallowa River within Diamond Prairie area. Image Derived from LiDAR Point Cloud colored by orthophotographs.*



## 9. Glossary

**1-sigma ( $\sigma$ ) Absolute Deviation:** Value for which the data are within one standard deviation (approximately 68<sup>th</sup> percentile) of a normally distributed data set.

**2-sigma ( $\sigma$ ) Absolute Deviation:** Value for which the data are within two standard deviations (approximately 95<sup>th</sup> percentile) of a normally distributed data set.

**Root Mean Square Error (RMSE):** A statistic used to approximate the difference between real-world points and the LiDAR points. It is calculated by squaring all the values, then taking the average of the squares and taking the square root of the average.

**Pulse Rate (PR):** The rate at which laser pulses are emitted from the sensor; typically measured as thousands of pulses per second (kHz).

**Pulse Returns:** For every laser pulse emitted, the Leica ALS 50 Phase II system can record *up to four* wave forms reflected back to the sensor. Portions of the wave form that return earliest are the highest element in multi-tiered surfaces such as vegetation. Portions of the wave form that return last are the lowest element in multi-tiered surfaces.

**Accuracy:** The statistical comparison between known (surveyed) points and laser points. Typically measured as the standard deviation ( $\sigma$ ) and root mean square error (RMSE).

**Intensity Values:** The peak power ratio of the laser return to the emitted laser. It is a function of surface reflectivity.

**Data Density:** A common measure of LiDAR resolution, measured as points per square meter.

**Spot Spacing:** Also a measure of LiDAR resolution, measured as the average distance between laser points.

**Nadir:** A single point or locus of points on the surface of the earth directly below a sensor as it progresses along its flight line.

**Scan Angle:** The angle from nadir to the edge of the scan, measured in degrees. Laser point accuracy typically decreases as scan angles increase.

**Overlap:** The area shared between flight lines, typically measured in percents; 100% overlap is essential to ensure complete coverage and reduce laser shadows.

**DTM / DEM:** These often-interchanged terms refer to models made from laser points. The digital elevation model (DEM) refers to all surfaces, including bare ground and vegetation, while the digital terrain model (DTM) refers only to those points classified as ground.

**Real-Time Kinematic (RTK) Survey:** GPS surveying is conducted with a GPS base station deployed over a known monument with a radio connection to a GPS rover. Both the base station and rover receive differential GPS data and the baseline correction is solved between the two. This type of ground survey is accurate to 1.5 cm or less.

## 10. Citations

Soininen, A. 2004. TerraScan User's Guide. TerraSolid.

## Appendix A

### LiDAR accuracy error sources and solutions:

Type of Error	Source	Post Processing Solution
GPS (Static/Kinematic)	Long Base Lines	None
	Poor Satellite Constellation	None
	Poor Antenna Visibility	Reduce Visibility Mask
Relative Accuracy	Poor System Calibration	Recalibrate IMU and sensor offsets/settings
	Inaccurate System	None
Laser Noise	Poor Laser Timing	None
	Poor Laser Reception	None
	Poor Laser Power	None
	Irregular Laser Shape	None

### Operational measures taken to improve relative accuracy:

1. Low Flight Altitude: Terrain following is employed to maintain a constant above ground level (AGL). Laser horizontal errors are a function of flight altitude above ground (i.e., ~ 1/3000<sup>th</sup> AGL flight altitude).
2. Focus Laser Power at narrow beam footprint: A laser return must be received by the system above a power threshold to accurately record a measurement. The strength of the laser return is a function of laser emission power, laser footprint, flight altitude and the reflectivity of the target. While surface reflectivity cannot be controlled, laser power can be increased and low flight altitudes can be maintained.
3. Reduced Scan Angle: Edge-of-scan data can become inaccurate. The scan angle was reduced to a maximum of  $\pm 14^\circ$  from nadir, creating a narrow swath width and greatly reducing laser shadows from trees and buildings.
4. Quality GPS: Flights took place during optimal GPS conditions (e.g., 6 or more satellites and PDOP [Position Dilution of Precision] less than 3.0). Before each flight, the PDOP was determined for the survey day. During all flight times, a dual frequency DGPS base station recording at 1-second epochs was utilized and a maximum baseline length between the aircraft and the control points was less than 19 km (11.5 miles) at all times.
5. Ground Survey: Ground survey point accuracy (i.e. <1.5 cm RMSE) occurs during optimal PDOP ranges and targets a minimal baseline distance of 4 miles between GPS rover and base. Robust statistics are, in part, a function of sample size (n) and distribution. Ground survey RTK points are distributed to the extent possible throughout multiple flight lines and across the survey area.
6. 50% Side-Lap (100% Overlap): Overlapping areas are optimized for relative accuracy testing. Laser shadowing is minimized to help increase target acquisition from multiple scan angles. Ideally, with a 50% side-lap, the most nadir portion of one flight line coincides with the edge (least nadir) portion of overlapping flight lines. A minimum of 50% side-lap with terrain-followed acquisition prevents data gaps.
7. Opposing Flight Lines: All overlapping flight lines are opposing. Pitch, roll and heading errors are amplified by a factor of two relative to the adjacent flight line(s), making misalignments easier to detect and resolve.